

DESIGN, CONSTRUCTION, AND INITIAL TEST OF HIGH SPATIAL RESOLUTION THERMOMETRY ARRAYS FOR DETECTION OF SURFACE TEMPERATURE PROFILES ON SRF CAVITIES IN SUPERFLUID HELIUM*

A. D. Palczewski[†], G. Ereamev, and R. L. Geng

SRF Institute, Jefferson Lab, 12000 Jefferson Ave. Newport News, VA 23606, USA

Abstract

We designed and built two prototype high resolution (0.6-0.55mm spatial resolution [1.1-1.2mm separation]) thermometry arrays out of Allen Bradley 90-120 ohm 1/8 watt resistors to measure local surface temperature profiles on SRF cavities. One array was designed to be physically flexible and conform to any location on a SRF cavity; the other was modeled after the common G-10/Stycast 2850 thermometer and designed to fit on the equator of an ILC (TESLA 1.3 GHz) cavity. We will discuss the advantages and disadvantages of each array and their construction. In addition we will present a case study of the arrays performance on a real SRF cavity TB9NR001. TB9NR001 presented a unique opportunity to test the performance of each array as it contained a dual (4mm separation) defect which conventional methods such as OST (Oscillating Superleak Transducers) and full coverage thermometry mapping were unable to resolve. We will discuss the new arrays' ability to distinguish between the two defects and their preheating performance.

INTRODUCTION

Modern superconducting radio frequency (SRF) cavities for use in particle accelerators are often limited below the theoretical limit by a single defect. There are three common techniques used in the SRF to ascertain the quench location; these include pass band measurements, OST (Oscillating Superleak Transducers) [1], and thermometer mapping [2]. Modern thermometry systems are broken into two categories; fixed thermometry systems [3–6] and rotation thermometry systems [7, 8]. Each system type has its limitation: fixed thermometry for instance have a spatial resolution of about 1 in, yet very sensitive temperature resolution; rotating thermometry systems have in theory infinite latitudinal resolution but low temperature sensitivity. While all these systems can give one the approximate location of the defect, they are not designed to distinguish between closely packed defects or give understanding about the defect in terms of local heat flux and heating profile.

* Authored by Jefferson Science Associates, LLC under U.S. DOE Contract No. DE-AC05-06OR23177. The U.S. Government retains a non-exclusive, paid-up, irrevocable, world-wide license to publish or reproduce this manuscript for U.S. Government purposes.

[†] ari@jlab.org

In an effort to gain higher spatial resolution without sacrificing the sensitivity of a fixed system, we designed and tested two prototype high spatial resolution thermometry arrays. These are the first step in moving from a thermometry mapping system to a calibrated calorimetry system which will give us the local heat flux and heating profile of a defect and its exact location. In this paper we describe the design, construction and initial test of two high resolution thermometry arrays, one flexible to fit any radius of a cavity and the second with a fixed radius matching a standard ILC cavity on the equator. Both arrays were able to identify the quench defect in TB9NR001 which had two cat-eye defects 4mm apart, the fixed array showed better thermal isolation, and therefore is a better candidate for calorimetry measurement in the future.

ARRAY DESIGN AND CONSTRUCTION

One of the initial goals of the project was to gain as high a spatial resolution as possible while keeping the $(T \cdot dR)/(R \cdot dT) \approx 4$ (1.4 to 4K) comparable with the current thermometry system at JLab [5, 9]. Keeping with the same resistive element, i.e., Allen Bradley 100 Ohm 1/8 watt (AB100Ω) carbon composite resistors was the logical choice.



Figure 1: Preparation of AB100Ω resistors for arrays. The top is the original and the bottom is modified for the arrays. See description in the text.

Preparation of Resistors for the Arrays

In order to archive the smallest possible resolution, the sides of the resistors needed to be ground down (to improve the packing ratio (Figure 1)). The grinding was performed using a 3 axis milling machine and a dermal cut off wheel disk. The resistors were held in place with bees wax to reduce stress on the element. One side was then ground flat until the resistive element was exposed; then the wax was

melted, the resistor flipped over and ground on the other side. This grinding process took the resistor from 1.6 mm diameter to 0.9 mm width. In addition to reducing the resistor width, the lead also needed to be replaced. The lead replacement served two purposes; one, to improve the thermal isolation (replacing copper with Manganin) and two, to make wiring more manageable as the new leads are more flexible and longer.

Flexible Array - Dow Corning Sylgard 184 Silicone Encapsulant

The first thermometry prototype array was designed out of 10 – AB100 Ω cast into an array with Dow Corning Sylgard 184 silicone encapsulant (Figure 2 left). Each resistor was modified according to the last subsection and mounted into the custom mill aluminum mold (one side of mold in shown in Figure 2 right). The aluminum mold consisted of multiple $0.95 \pm 0.05\text{mm}$ channels with $0.1 \pm 0.05\text{mm}$ spacing on a radius which is identical to the outer surface of a ILC cavity ($r = 106 \pm 1\text{mm}$ [10]). After casting, the cavity side of the 10 element array were ground down to expose the resistive carbon and then the elements were covered in GE varnish to ensure electrical isolation, similar to the standard AB100 thermometers [3, 5].

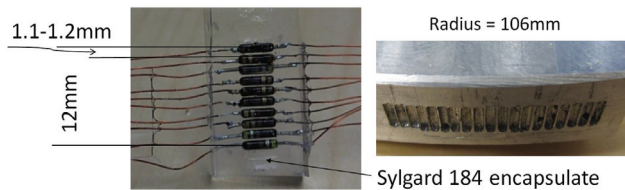


Figure 2: Flexible high resolution thermometry prototype 1 (left) and one side of aluminum mold which created the array (right).

Fixed Radius Array - G10/Stycast 2850 Encapsulant

The second thermometry prototype array was designed out of 13 – AB(90-120) Ω resistors fixed into a G10 board and cast with Stycast 2850 (Figure 3). Unlike the first prototype, which need a mold, the second prototype was milled out of a solid piece of G10. A 106 mm arc was milled into the G10, and the 13 (1 mm \times 4 mm \times 1 mm) trenches were placed on the surface. At both ends of each trench a 1 cm hole was drilled perpendicular to the trench in order to thread the leads through. At the bottom of the drill holes, a trench was made to the outside so the leads could be pulled out side of the g10 board. After the resistor were placed in the trench and the leads pulled through, the holes and trenches were filled in with Stycast 2850 Figure 3 – right. After drying the extra Stycast was removed down to the carbon elements of the resistors, and GE varnish was painted over the exposed elements for electrical isolation.

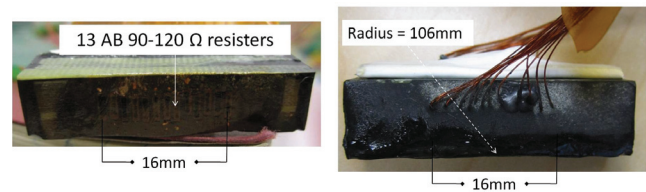


Figure 3: Fixed high resolution thermometry prototype 2: front (left) and side (right) profile. The array consists of 13 90-120 Ω resistors fixed in a g10 board with 106mm arc.

TESTING ON TB9NR001

We chose to test our new arrays on TB9NR001 because of the cavity's unique quench limiting defect at 17.3MV/m. Prior to testing the arrays, TB9NR001 was tested using OST, and full cell thermometry mapping, which identified a localized limiting quench in cell 5 on the equator close to 25° (we follow standard ILC definition of angle orientation on the cavity). Optical inspection with JLab's high resolution cavity inspection tool [11] revealed cell 5 actually had two cat-eye defects on the equator which were spaced 3.8mm apart (Figure 4 left). One defect is 330 μm in diameter (major) and other is 230 μm (minor). The initial thermometry mapping defect is shown in Figure 4 right (black hand written circle). To unsure we had the proper location we modified the current JLab optical inspection tool with a calibrated laser system to find the defect location (Figure 4 right red dot).

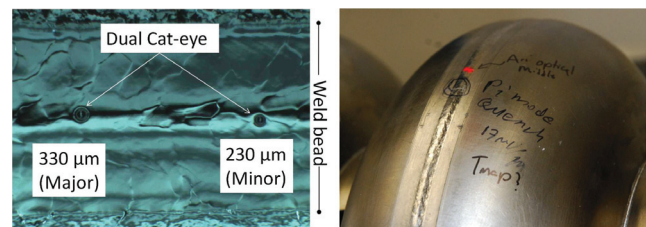


Figure 4: Dual cat-eye defect cell 5 TB9NR001. Left – internal inspection with JLab's high resolution optical inspection machine. Right – external view of cell. See text for detailed description.

Thermometry Mounting

After the identification of the dual defect location on the outside of the cavity, the thermometry arrays were mounted to the cavity for testing. We used the current JLab ILC thermometry mounting brackets [5] to secure each array to the cavity (Figure 5). Each array was thermally anchored to the cavity with Apiezon–N grease, and backed with Gore-tex tape to help distribute the pressure from the bracket. Enough pressure was applied to ensure most of the grease squeezed out of the gap between the cavity and the arrays;

the pressure was not calibrated. The flexible array was centered on the middle of the two defects, while the fixed array was centered on the major defect.

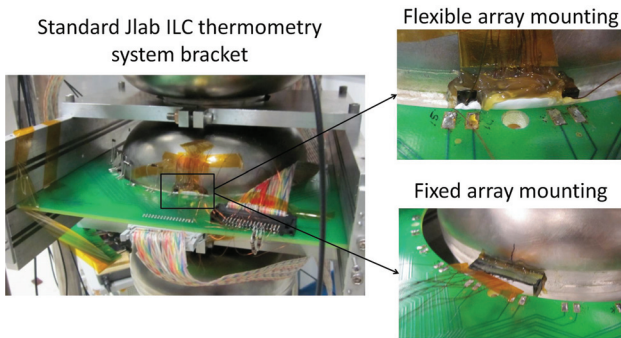


Figure 5: Thermometry array mounting on NR1 cell 5. Both arrays were mounted in the same way on the left, the zoom in of each array is on the right; flexible on top and fixed radius on bottom.

Flexible Array Performance

The performance of the flexible array to distinguish between the defects is shown in Figure 6. The top graph shows the temperature profile (temperature raise above the 1.8K LHe bath) for the array at multiple fixed field levels. The end resistors at -10 mm and 14 mm are standard JLab thermometers. The small insert at the bottom of the picture is the approximate location ($\pm 0.6\text{mm}$) of the dual defects on the inside of the cavity. Each color/symbolled curve is at a constant fixed field. The graph clearly shows the major defect is the dominate defect in the system although it appears the minor defect may also show some preheating. The bottom graph shows the preheating profile temperature vs. H^2 before the quench field. Each colored and symbolled line represents an individual thermometer in the array, the two black line are from conventional thermometers set at the ends of the array. From 5000 mT^2 (16.7 MV/m) to 5270 mT^2 (17.15 MV/m) the defects show quadratic heating, and from 5270 mT^2 (17.15 MV/m) to 5375 mT^2 (17.3 MV/m) quench shows exponential heating. Below 4700 mT^2 (16.2 MV/m) the flexible array showed no sign of preheating. One can see the thermal isolation of the standard thermometer (-10 mm and 14 mm) is much higher than flexible array as the change in temperature is larger than most of the array even though they are farther away from the defects, in addition preheating signature started below 4 MV/m (not shown).

Fixed Radius Array Performance

The performance of the fixed radius array to distinguish between the defects is shown in Figure 7. The top graph shows the temperature profile (temperature above the 1.8K bath) for the array at multiple fixed field. The small insert

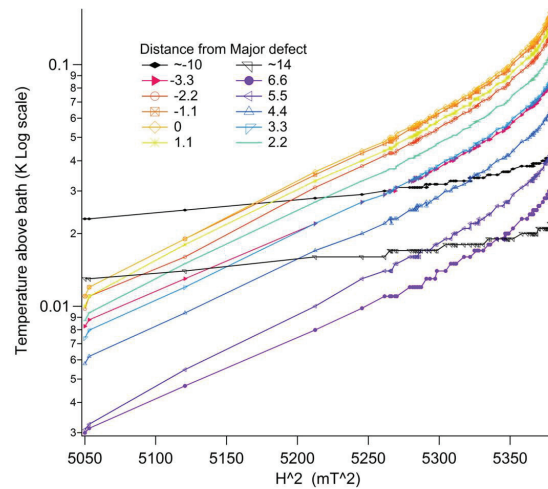
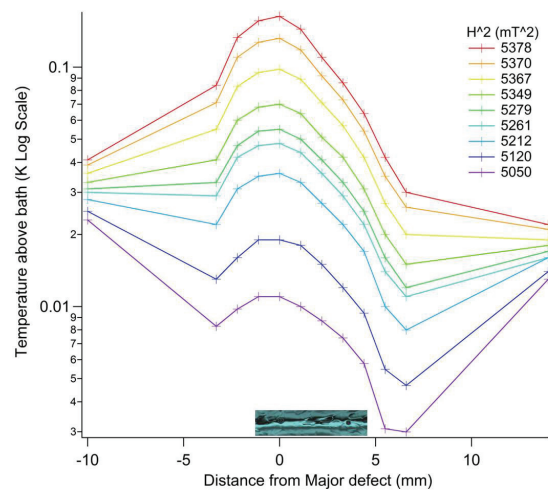


Figure 6: Flexible thermometry test on TB9NR001. Top – Array profile (temperature (log scale) vs. position) each curve is from a fixed field. Bottom – Preheating profile (temperature (log scale) vs. H^2) before quench. See text for details.

at the bottom is the approximate location ($\pm 0.6\text{mm}$) of the dual defect on the inside of the cavity. Each color/symbolled curve is at a constant fixed field. The graph clearly shows the major defect is the dominate defect in the system although it appears the minor defect also shows some small preheating. The bottom graph shows the preheating profile temperature vs. H^2 before a quench. Each colored and symbolled line represents an individual thermometer in the array. Unlike the first test with the flexible array preheating, the fixed array preheating started almost immediately (218 mT^2 or 4MV/m). Initially the heating was quadratic (Joule heating) until about 3800 mT^2 (14.5MV/m) although the resistor close to the major defect start to change around 2500 mT^2 (11.8MV/m). After 3800 mT^2 the slope becomes higher and then turns exponential with the thermometers close to the major defect deviating the most from linear. Although one would expect the major defect to have

higher preheating temperature at all fields – as it is the quenching defect. Below 4200 mT^2 (15.3 MV/m) the minor defect appears to produce more heat. Another item to note, although the distance between the defects in the cavity is 3.8 mm , the two peaks close to the quench field are closer to 5 mm .

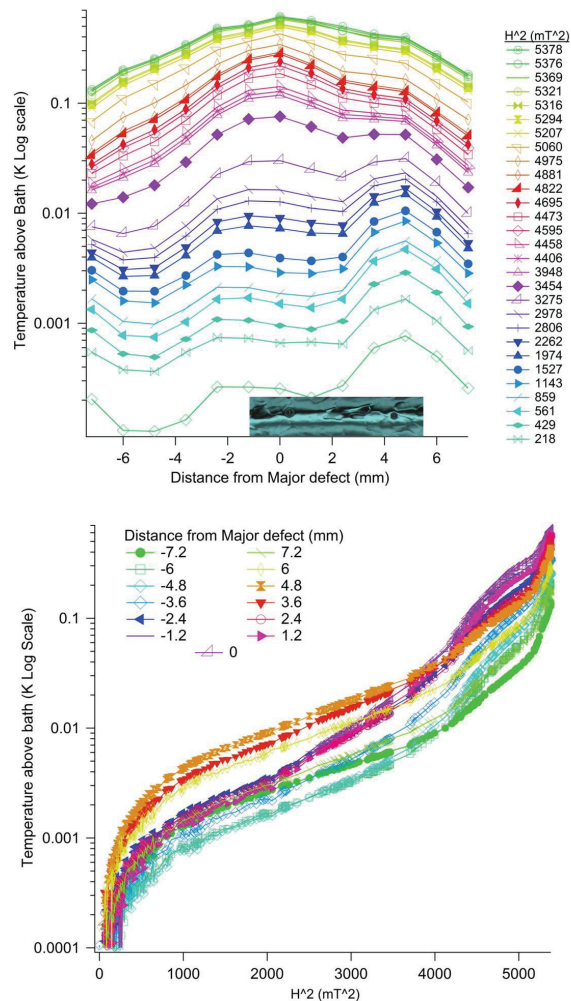


Figure 7: Fixed radius thermometry test on TB9NR001. Top – Array profile (temperature (log scale) vs. position) each curve is from a fixed field. Bottom – Preheating profile (temperature (log scale) vs. H^2) before quench. See text for details.

CONCLUSION

We designed and built two prototype high resolution thermometry arrays to measure local surface temperature profiles on SRF cavities. The two new prototypes were tested on the dual defects in cell five of TB9NR001. The new prototype arrays we were able to determine that the larger of two cat-eye pits was the limiting defect in TB9NR001. Each array found the heating profile deviated from quadratic (Joule heating) although at different

fields. The fixed radius array was clearly superior in terms of thermal isolation - either due to the casting compound, or the fact that the leads were better isolated in the fixed array. The fixed radius array design is a viable candidate for calorimetry measurements in the future.

REFERENCES

- [1] Z. A. Conway, D. L. Hartill, H. S. Padamsee, and E. N. Smith, Proceedings of LINAC08 THP036, 863, Victoria, British Columbia, Canada (2008).
- [2] C. M. Lyneis, M. McAshen, and N. T. Viet, Proceedings of the 1972 Proton Linear Accelerator Conference, 98, Los Alamos, NM, USA (1972).
- [3] J. Knobloch, H. Muller, and H. Padamsee, Review of Scientific Instruments **65**, 3521 (1994).
- [4] Darryl Orris, Leo Bellantoni, Ruben H. Carcagno, Helen Edwards, Elvin Robert Harms, Timergali N. Khabiboulline, Sergey Kotelnikov, Andrzej Makulski, Roger Nehring, and Yuriy Pischalnikov, Proceedings of PAC07, WEPMN105 2280, Albuquerque, New Mexico, USA (2007).
- [5] G. Ciovati, Flood R, Kneisel P, Machie D, and Morrone M, Jefferson Nation laboratory technical notes, JLAB-TN-08-012 (2008).
- [6] A. Canabal, J.D. Bowyer, P. Chacon, N. A. Gillespie, M.A. Madrid, and T. Tajima, Proceedings of PAC07, WEPMS031 2406, Albuquerque, New Mexico, USA (2007).
- [7] Q. S. Shu, G. Deppe, W-D. Moeller, M. Pekeler, D. Proch, D. Renken P. Stein, C. Stolzenburg, T. Junquera, A. Caruette, and M. Fouaidy, Proceedings of PAC95, TPP11 1639, Dallas, Texas, USA (1996).
- [8] Hiroshi Sakai, Takaaki Furuya, Takeshi Takahashi, Shogo Sakanaka, Kensei Umemori, Proceedings of IPAC10, WEPEC028 2950, Kyoto, Japan (2010).
- [9] J. Knobloch, Dissertation, Cornell University (1997).
- [10] N. Juntong, R.M. Jones, and I.R.R. Shinton, arXiv:0906.3592v1 (2009).
- [11] R. L. Geng, and T. Goodman, Proceedings of SRF2011, THPO036 to be published, Chicago Illinois, USA (2011).